Free vibration analysis of Three-Phase CNT/ Polymer/Fiber Laminated Tow-Steered Quadrilateral Plates considering Agglomeration Effects

Jamshid Fazilati[a], Vahid Khalafi[b], Meisam Jalalvand[c]

[a] *Aeronautical Science and Technology Department, Aerospace Research Institute, Mahestan St., 14657-74111 Tehran, Iran*

[b] *Aerospace Engineering Department, Shahid Sattari Aeronautical University of Science and Technology, Tehran, Iran*

[c] *Engineering Materials, School of Engineering, University of Southampton, SO17 1BJ Southampton, United Kingdom*

Abstract

This paper introduces a numerical model for predicting the properties of the tow-steered three-phase CNT/polymer/fiber composition. The free vibration of laminated quadrilateral plates is addressed. The behavior of the matrix reinforced with the carbon-nanotube (CNT) additive is calculated based on the Eshelby-Mori-Tanaka micromechanics approach. The approach considers the probable agglomerated CNT phases in the mixture. Every lamina of the laminate is assumed to be constructed by the curvilinear fiber arrangement dipped in the nanocomposite matrix. The fiber placement paths follow smooth orientation angle changing routes. Several homogenization techniques are presented in detail to evaluate the overall properties of the tow-steered three-phase CNT/polymer/fiber laminate. The principle of virtual work based on the first-order shear deformation plate theory is implemented through the NURBS isogeometric analysis method. Some representative results are obtained and compared with those available in the literature to demonstrate the quality of the proposed formulation. The effects of problem variables including the layup, mixture quality, boundary condition, and micromechanical model on the free vibration behavior are investigated by performing parametric studies.

Keywords: CNT, Agglomeration, Eshelby-Mori-Tanaka scheme, Tow-steered, Three-Phase composition, IGA, Quadrilateral plate.

1. Introduction

The thin-walled composite structures are major structural elements, especially wherever the stiffness to weight ratio is a primary structural performance concern. A composite material may be built up by adding fibrous reinforcements or may reach by making some material components combination. A conventional fibrous-reinforced form of composite materials is laminated composites using prepreg or fiber fabrics. In the past two decades, there have been consecutive efforts to achieve higher and customized structural composites from the mechanical and physical behavior view of points. The improvements have been attained in mechanical and stiffness properties and other physical characteristics, including fracture, fatigue, thermal, and manufacturing processes. The development of modern fibers, fiber-placement technologies, and the introduction of nanocomposites are among the most important improving techniques in the case of polymer matrix composites. The CNT/polymer/fiber laminates, in conjunction with the curvilinear fiber placement technology, are introduced to provide high-performance structures avoiding both the matrix and delamination failure modes and the structural over-designs.

Carbon nanotubes (CNT), thanks to their special molecular structure, offer excellent mechanical properties, including extremely-high elastic modulus, high tensile strength, and good geometrical characteristics. The addition of CNTs with their exceptional mechanical properties to the polymer composites could bring great promising excellences while having almost no considerable effect on the structural weight. Therefore, the efficiency of the structure may improve without weight penalties. Weight efficiency is a primary goal, especially in aerial, space, and marine structural design. The evaluation of the overall mechanical properties of such materials may perform by using the constituent's characteristics through micromechanics models.

Due to the high strength-to-mass ratio of nano-particles/fiber-reinforced laminated polymer composites, they received significant attention in recent years [1-9]. Heshmati and Yas [10] investigated the free vibration of functionally graded (FG) beams reinforced with carbon nanotubes (CNT). The effect of nano-particle agglomeration and CNTs distribution was determined using the Eshelby-Mori-Tanaka approach. Bhardwaj et al. [11] calculated the nonlinear flexural and dynamic response of CNT-reinforced laminated

composite plates. The fast-converging finite double Chebyshev polynomials were utilized based on the first-order shear deformation theory (FST). The Halpin-Tsai approach was applied to evaluate the properties of the nano particle-reinforced matrix. Rafiee et al. [12] presented the nonlinear free vibration analysis of CNT/fiber/polymer composite plates with piezoelectric layers by FST Galerkin's method. The Halpin-Tsai scheme and the fiber micromechanics were used to predict the material properties assuming the carbon nanotubes were uniformly distributed and randomly oriented through the epoxy resin matrix. Kiani [13] calculated the natural frequencies of CNT-reinforced composites skew plates. The reinforcing CNT particles were assumed to be functionally distributed across the plate thickness. The FST Ritz method was implemented to extract the governing eigenvalue problem. An enhanced version of the rule of mixtures is utilized to predict the equivalent mechanical properties of the reinforced mixture. Ardestani et al. [14] investigated the bending and vibration behavior of CNT-reinforced composite skew plates by using the isogeometric method. Reddy's third-order shear deformation theory (TST) was applied. The effective mechanical properties were calculated by employing an extended rule of mixture. Kamarian et al. [15] performed the free vibration and optimization analysis of a three-phase CNT/polymer/fiber laminated plate by the FST generalized differential quadrature method (GDQM). The Mori-Tanaka (MT) approach and the firefly algorithm were applied. Tornabene et al. [16,17] studied the linear static behavior, and the free vibration of three-phase CNT/polymer/fiber laminated composite plates and shells. The agglomerated CNTs were considered through the Eshelby-Mori-Tanaka approximation through the GDQM formulation. Ghasemi et al. [18] studied the influences of the agglomeration and distribution patterns of the CNTs on the vibration behavior of CNT/fiber/polymer/metal hybrid laminated cylindrical shells using the Eshelby-Mori-Tanaka approach. Yousefi et al. [19] examined the effects of agglomeration on the free vibration behavior of truncated conical laminates. A three-phase CNT/polymer/fiber laminate assumed with the TST GDQM was employed. The material mixture properties were estimated using the rule of mixture and Eshelby-Mori-Tanaka mixed with Hahn's homogenization technique. Georgantzinos et al. [20] studied the buckling of nanocomposite rectangular plates using the finite element method (FEM) considering random dispersion, waviness, and agglomeration of CNTs. The rule of mixtures and the Halpin-Tsai model were

employed to calculate the elastic modulus of the nanocomposite matrix. Heidari and his colleagues [21] presented a numerical analysis of the nanocomposite buckling problem considering the mixture shortcomings such as non-straight CNTs, CNTs with atomic voids, and CNT aggregation based on the nonlocal theory. Craveiro et al. [22] investigated the influence of CNTs agglomeration on thick nanocomposite plates' behavior. The two-parameter model of agglomeration based on the Eshelby-Mori-Tanaka approach was implemented through the finite element method. Demir et al. [23] developed a continuum-based model of agglomerated nanocomposite with a statistical approach based on a modified three-phase Mori-Tanaka model.

The traditional composite laminate designs employ straight and uniformly spaced prepreg fibers or woven reinforcements. This design leads to unchanged directional lamina properties throughout the entire ply. Customized mechanical properties may be attained in fibrous composites by variable-oriented reinforcing fibers via automated fiber placement technology. Since the fiber orientation varies by location, the ply gains location-dependent directional stiffnesses through the geometry. So, a multi-ply composite of this kind is called variable stiffness composite laminate (VSCL). Another kind of VSCL may attain from the variation of either fiber spacing or fiber characteristics.

Akhavan and Ribeiro [24] studied the free vibration of polymer/fiber VSCL plates with curvilinear fibers using TST finite element method. Tornabene and co-workers [25] investigated higher-order structural theories for the static analysis of doubly curved polymer/fiber composite laminated panels reinforced by curvilinear fibers using the GDQM. They extracted the strain and stress distribution through the thickness direction. A review of the design for the manufacture of VSCL panels is reported by Lozano et al. [26]. Hao et al. [27,28] performed buckling analysis and layup optimization of the polymer/fiber VSCL plates containing circular cutouts by an isogeometric formulation based on the Reissner-Mindlin plate theory. Khalafi and Fazilati [29-30] investigated the supersonic panel flutter and parametric instability of tow-steered VSCL quadrilateral plates using a developed FST NURBS IGA formulation. They [31] also presented a free vibration analysis of the VSCL plate containing embedded perforations of various layouts using the FST-IGA formulation by implementing the Nitsche technique.

Based on the survey and to the best of the authors' knowledge, the mechanical behavior of three-phase CNT/polymer/fiber laminated panels with curvilinear fiber reinforcement is not addressed. In the present paper, a FST NURBS-based isogeometric formulation is utilized to investigate the mechanical behavior of the tow-steered three-phase CNT/polymer/fiber laminate quadrilateral plates. The free vibration behavior of the geometry subjected to various sets of boundary conditions is studied. The micromechanics of CNTs is based on the agglomeration model for randomly oriented CNTs presented by the Eshelby-Mori-Tanaka approach. Furthermore, five different homogenization techniques are examined and presented in detail in evaluating the overall elastic properties in terms of engineering constants of the tow-steered three-phase CNT/polymer/fiber laminate plate.

2. Problem formulation

2.1 Micromechanics of three-phase CNT/polymer/fiber laminated

A three-phase CNT/polymer/fiber laminated composite is a composition of CNT-reinforced polymer matrix and the wetted curvilinear fiber reinforcements. The three-phase composite consists of three main components: the polymer matrix resin, the additives of carbon nanotubes, and the reinforcing fibers (Fig. 1).

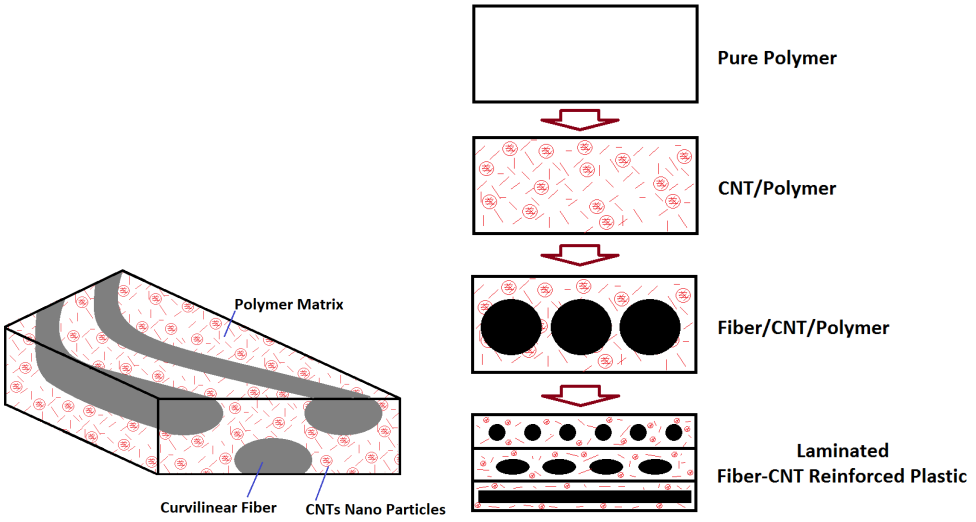

Fig. 1. Schematic views of three-phase fiber /CNT/polymer composite with curvilinear fibers

A two-step procedure is applied to evaluate the overall mechanical properties of the complete structure of the three-phase CNT/polymer/fiber laminated composite as illustrated in Fig. 2. First, the mechanical properties of the polymer matrix reinforced by carbon nanotubes are calculated. The implemented Eshelby-Mori-Tanaka (EMT) model [16] enables considering of possible particle clustering effects. The two-phase nanocomposite is further supported with dipped reinforcing fibers. At this step, several fiber-matrix micromechanical models, including the rule of mixture model [32,15], Hahn model [33], Halpin-Tsai model [16], and Mori-Tanaka model [34], are employed and evaluated.

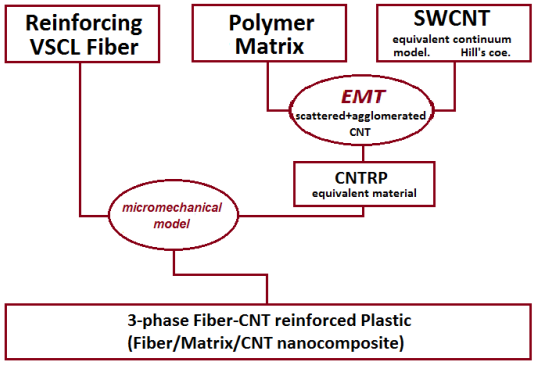

Fig. 2. Hierarchy of the three-phase CNTs/fiber/polymer multiscale composite constituent phases.

2.2 Equivalent properties of CNT enriched matrix:

The polymer matrix medium is isotropic and fully characterized by its elastic modulus, Poisson's ratio, and density (i.e., E_m, υ_m, ρ_m). The CNT mixing process conventionally leads to some agglomerated spots of CNT bunches in the mixture (Fig. 3).

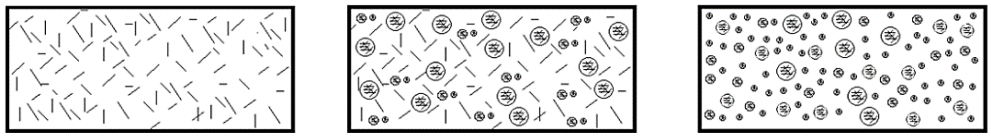

no agglomeration, fully scattered
$\mu = \eta = 1$

semi-agglomerated
$\mu<\eta\ ,\ \eta < 1$

fully agglomerated
$\mu<\eta\ ,\ \eta = 1$

Fig. 3. SEM images of the CNT nanocomposite films and the idealization of the mixture; (a) fully scattered mixture; (b) partially clustered particles; (c) almost fully clustered particles [7]

Hill's elastic moduli constants denote the CNT estimated mechanical properties (i.e., $k_r, l_r, m_r, n_r, p_r, \rho_r$). It is also assumed that the CNT nano-particles and inclusions are well-mixed in the polymer medium (i.e. uniformly distributed). The total volume of the mixture, *W*, may be calculated from the volume size of the inclusions (W_r^{cnt}), the volume of the scattered CNTs (W_r^{inc}), and the involving medium (W_m) as [17],

$$W = W_m + (W_r^{inc} + W_r^{cnt}) \tag{1}$$

The volume fraction of reinforcing CNT content, V_r, could be calculated as a function of mixture mass ratio (w_r) and the mixture constituent's densities as,

$$\frac{1}{V_r} = \frac{\rho_r}{w_r \cdot \rho_m} - \frac{\rho_r}{\rho_m} + 1 \tag{2}$$

w_r is the total nano-phase additives mass ratio to the mixture mass. Two mixing parameters (i.e., (μ,η)) are introduced to characterize the rate and dominance state of the inclusions against scattered CNTs in the mixture [17].

$$\mu = \frac{V^{in}}{V},\ \eta = \frac{V_r^{in}}{V_r} \qquad \left\{\forall\, \mu \le \eta,\ \mu,\eta \in [0,1]\right\} \tag{3}$$

The μ parameter defines the fraction of the volume of the particle clusters (V^{in}) to the total volume of the nanocomposite (V). The η parameter indicates the volume of CNTs trapped in the clusters (the agglomerated portion of CNTs, V_r^{in}) to the total CNT volume (V_r). The condition of uniformly well-mixed

CNTs with no clusters is expressed as $\mu = \eta = 1$. With clusters, the parameters are indexed as $\mu < \eta \leq 1$ which, in the case of totally agglomerated inclusions, η reaches 1. These conditions are graphically illustrated in Fig. 3.

According to the EMT scheme, the bulk and shear modulus is now calculated for both inside the spherical inclusions (K_{inc}, G_{inc}) and the polymer medium embedded with scattered CNTs (K_{cntrp}, G_{cntrp}) as [16],

$$\begin{aligned} K_{inc} &= K_m + \frac{\varepsilon \eta V_r - 3\alpha \eta V_r K_m}{3\mu - 3\eta V_r + 3\alpha \eta V_r} \qquad & K_{cntrc} &= K_m + \frac{V_r(1-\eta)(\varepsilon - 3\alpha K_m)}{3(1-\mu-(1-\eta)V_r + \alpha(1-\eta)V_r)} \\ G_{inc} &= G_m + \frac{\gamma \eta V_r - 2\beta \eta V_r G_m}{2\mu - 2\eta V_r + 2\beta \eta V_r} & G_{cntrc} &= G_m + \frac{V_r(1-\eta)(\gamma - 3\beta G_m)}{2(1-\mu-(1-\eta)V_r + \beta(1-\eta)V_r)} \end{aligned} \tag{4}$$

in which G_m, K_m are the shear and bulk moduli of the isotropic matrix and can be evaluated as

$$\begin{aligned} K_m &= \frac{E_m}{3(1-2\nu_m)} \\ G_m &= \frac{E_m}{2(1+\nu_m)} \end{aligned} \tag{5}$$

Where E_m, ν_m are the elastic modulus and Poisson's ratio of the pure matrix. By using the CNT approximated Hill's mechanical constants, the dimension-less material coefficients $\alpha, \beta, \varepsilon, \gamma$ are introduced as,

$$\begin{aligned} \alpha &= \frac{3K_m + 3G_m + k_r + l_r}{3G_m + 3k_r} \\ \beta &= \frac{1}{2}\left(\frac{4G_m + 2k_r + l_r}{3G_m + 3k_r} + \frac{4G_m}{G_m + p_r} + \frac{6G_m K_m + 2G_m^2 + 3G_m K_m + 7G_m^2}{3G_m K_m + G_m^2 + 3m_r K_m + 21 m_r G_m} \right) \\ \varepsilon &= \frac{1}{3}\left(n_r + 2l_r + \frac{(2k_r + l_r)(3K_m + G_m - l_r)}{G_m + k_r} \right) \\ \gamma &= \frac{1}{5}\left(\frac{2n_r - 2n_r}{3} + \frac{8G_m p_r}{G_m + p_r} + \frac{2(k_r - l_r)(2G_m + l_r)}{3G_m + 3k_r} + \frac{24 m_r G_m K_m + 32 m_r G_m^2}{3m_r K_m + 3G_m K_m + 7m_r G_m + 7G_m^2} \right) \end{aligned} \tag{6}$$

In which $(k_r, l_r, m_r, n_r, p_r)$ are five independent constants known as Hill's elastic moduli constants [16].

The equivalent mechanical properties of the CNT-matrix mixture medium are defined according to the EMT model as,

$$E_m^* = \frac{9\,K_m^*\,G_m^*}{3K_m^* + G_m^*} \quad , \quad \nu_m^* = \frac{3\,K_m^* - 2\,G_m^*}{6K_m^* + 2\,G_m^*} \quad , \quad \rho_m^* = \rho_m V_m + \rho_r V_r \;\; (V_m + V_r = 1) \tag{7}$$

The subscripts $_m$ and $_r$ stand for the matrix and reinforcement components. The density is calculated by the simple rule of mixture. ρ and V are the density and volume fractions, respectively. The effective bulk and shear modulus of the matrix filled with scattered and agglomerated phases of the CNT additives are expressed as [16],

$$\begin{aligned} K_m^* &= K_{cntrp}\left(1+\frac{\mu\,K_{rel}\text{-}\mu}{1+(1\text{-}\mu)(K_{rel}\text{-}1)(1+\upsilon_{cntrp})/(3\,\upsilon_{cntrp}\text{-}3\,\upsilon_{cntrp})}\right) \\ G_m^* &= G_{cntrp}\left(1+\frac{\mu\,G_{rel}\text{-}\mu}{1+(1\text{-}\mu)(G_{rel}\text{-}1)(8\text{-}10\,\upsilon_{cntrp})/(15\text{-}15\,\upsilon_{cntrp})}\right) \\ \left(K_{rel}=\frac{K_{inc}}{K_{cntrp}}, G_{rel}=\frac{G_{inc}}{G_{cntrp}}, \upsilon_{cntrp}=\frac{3K_{cntrp}\text{-}2G_{cntrp}}{6K_{cntrp}+2G_{cntrp}}\right) \end{aligned} \tag{8}$$

The asterisk superscript refers to the mechanical properties of the two-phase CNT-embedded polymer matrix.

2.3 Equivalent properties of CNTRP reinforced with curvilinear fibers:

The CNT-reinforced plastic matrix (CNTRP) is supposed to be isotropic and fully characterized by its elastic modulus, Poisson's ratio, and density properties (i.e., $E_m^*, \upsilon_m^*, \rho_m^*$) according to Eq (7). The fiber reinforcements' mechanical properties are radial orthotropic. They could be fully expressed with main and transverse elastic modulus, main-transverse and transverse-transverse shear modulus, main Poisson's ratio,

and density parameters (i.e., $E_f^{11}, E_f^{22}, G_f^{12}, G_f^{23}, \upsilon_f^{12}, \rho_f$). The parameter V_f is assumed as the volume fraction of fibers to the total lamina volume.

The resulting mechanical properties of the composition of the isotropic two-phase reinforced matrix and the curvilinear fibers (i.e., the three-phase CNT/polymer/fiber composite lamina) are derived. Five different micromechanical schemes are implemented, including the models of the rule of mixture, Hahn, Halpin-Tsai, and Mori-Tanaka. These models are introduced in the following.

2.3.1 Rule of mixtures model I:

Using the rule of mixture for estimating the directional mechanical properties of long unidirectional fibers dipped in the isotropic matrix gives the following relationships [32],

$$\begin{cases} E_1 = E_{1f}V_f + E_m^*V_m^* \\ {E_2}^{-1} = {E_{2f}}^{-1}V_f + {E_m^*}^{-1}V_m^* \\ {G_{12}}^{-1} = {G_{12f}}^{-1}V_f + {G_m^*}^{-1}V_m^* \\ {G_{23}}^{-1} = {G_{23f}}^{-1}V_f + {G_m^*}^{-1}V_m^* \\ \nu_{12} = \nu_{12f}V_f + \nu_m^*V_m^* \end{cases} \tag{9}$$

The subscript $_f$ specifies the material properties of the fiber phase.

2.3.2 Rule of mixtures model II:

An improved rule of mixture formulation with minor modifications is presented as [15]:

$$\begin{cases} E_1 = E_{1f}V_f + E_m^*V_m^* \\ {E_2}^{-1} = {E_{2f}}^{-1}V_f + {E_m^*}^{-1}V_m^* + R \\ {G_{12}}^{-1} = {G_{12f}}^{-1}V_f + {G_m^*}^{-1}V_m^* \\ {G_{23}}^{-1} = {G_{23f}}^{-1}V_f + {G_m^*}^{-1}V_m^* \\ \nu_{12} = \nu_{12f}V_f + \nu_m^*V_m^* \end{cases} \tag{10}$$

$$(R = V_fV_m^* \frac{{\nu_{12f}}^2 E_m^* \,/\, E_{2f} + {\nu_m^*}^2 E_{2f} \,/\, E_m^* - 2\nu_{12f}\nu_m^*}{V_fE_{2f} + V_m^*E_m^*})$$

2.3.3 Mori-Tanaka model:

According to the Mori-Tanaka micromechanical model, the average stress and strain of the constituent fiber and the matrix are correlated in a composite ply. The directional properties of unidirectional fiber composite based on Mori-Tanaka assumptions may calculate through [34],

$$\begin{cases} E_1 = \dfrac{(A_{11}+A_{22}+A_{32})V_f V_m^* + (A_{11}(A_{22}+A_{32})-2A_{21}A_{12})V_m^{*2} + {V_f}^2}{V_f V_m^*(2A_{21}({S_{12m}}^* - {S_{12}}^f) + (A_{22}+A_{32}){S_{11}}^f + A_{11}{S_{11m}}^*) + (A_{11}(A_{22}+A_{32})-2A_{12}A_{21}){S_{11m}}^* V_m^{*2} + {S_{11}}^f {V_f}^2} \\ E_2 = \dfrac{((A_{22}-A_{32})V_m^* - V_f)((A_{11}+A_{22}+A_{32})V_f V_m^* + (A_{11}(A_{22}+A_{32})-2A_{12}A_{21})V_m^{*2} + {V_f}^2)}{A_{22}(b_1+b_2)V_m^* + A_{12}(b_3+b_4)V_m^* + b_5(A_{11}V_m^* + V_f) + {A_{22}}^2 {S_{11m}}^* V_m^{*2}(A_{11}V_m^* + V_f)} \\ G_{12} = \dfrac{(V_f + V_m^* A_{66}){G_{12}}^f G_m^*}{V_f G_m^* + V_m^* A_{44}{G_{12}}^f} \\ G_{23} = \dfrac{(V_f + V_m^* A_{44}){G_{23}}^f G_m^*}{V_f G_m^* + V_m^* A_{44}{G_{23}}^f} \\ \nu_{12} = \dfrac{A_{12}V_m^*(V_f({S_{11}}^f - {S_{11m}}^*) + 2A_{21}V_m^* {S_{12m}}^*) - (V_f + A_{11}V_m^*)(V_f {S_{12}}^f + (A_{22}+A_{32})V_m^* {S_{12m}}^*)}{{V_f}^2 {S_{11}}^f + (-2A_{12}A_{21} + A_{11}(A_{22}+A_{32}))V_m^{*2}{S_{11m}}^* + V_f V_m^*((A_{22}+A_{32}){S_{11}}^f + A_{11}{S_{11m}}^* + 2A_{21}(-{S_{12}}^f + {S_{12m}}^*))} \end{cases} \quad (11)$$

Where

$$\begin{aligned} b_1 &= V_f V_m^* \left\{ A_{12}({S_{12m}}^* - {S_{12}}^f) + A_{11}({S_{22}}^f - {S_{11m}}^*) \right\} \\ b_2 &= {V_f}^2 (S_{22}^f + {S_{11m}}^*) - 2A_{12}A_{21}{S_{11m}}^* V_m^{*2} \\ b_3 &= A_{21}V_m^* \left\{ 2A_{32}{S_{11m}}^* V_m^* - V_f({S_{22}}^f - {S_{23}}^f + {S_{11m}}^* + {S_{12m}}^*) \right\} \\ b_4 &= V_f V_m^* \left\{ A_{12}({S_{12m}}^* - {S_{12}}^f) + A_{11}({S_{22}}^f - {S_{11m}}^*) \right\} \\ b_5 &= A_{32}V_f {V_m}^*({S_{12m}}^* - {S_{23}}^f) - {A_{32}}^2 {S_{11m}}^* V_m^{*2} + {S_{12}}^f {V_f}^2 \end{aligned} \quad (12)$$

The components of the 3-D Mori-Tanaka bridging matrix (A) and material compliance matrices (S) are defined according to [35].

2.3.4 Hahn model:

The elastic moduli, shear moduli, and Poisson's ratios of a three-phase CNT/polymer/fiber composite can be calculated using the homogenization technique proposed by Hanh et al. [33] as follows:

$$\begin{cases} E_1 &= E_{1f}V_f + E_m^*V_m^* \\ E_2 &= \dfrac{4E_1K_TG_{23}}{E_1K_T + G_{23}(E_1 + 4K_T\nu_{12}^2)} \\ G_{12} = G_{13} &= \dfrac{V_f + \Delta_1V_m^*}{V_f \,/\, G_{12f} + \Delta_1V_m^* \,/\, G_m^*} \\ G_{23} &= \dfrac{V_f + \Delta_2V_m^*}{V_f \,/\, G_{23f} + \Delta_2V_m^* \,/\, G_m^*} \\ \nu_{12} &= \nu_{12f}V_f + \nu_m^*V_m^* \end{cases} \tag{13}$$

Where

$$\begin{aligned} \Delta_1 &= \frac{1}{2}(1 + G_m^* \,/\, G_{12f}) \\ \Delta_2 &= \frac{1}{4}(3 - 4\nu_m^* + G_m^* \,/\, G_{23f}) \,/\, (1 - \nu_m^*) \\ \Delta_k &= \frac{1}{2}(1 + G_m^* \,/\, K_f) \,/\, (1 - \nu_m^*) \\ K_T &= (V_f + \Delta_kV_m^*) \,/\, (V_f \,/\, K_f + \Delta_kV_m^* \,/\, K_m^*) \\ K_f &= E_{22f} \,/\, 3(1 - 2\nu_{23f}) \end{aligned} \tag{14}$$

2.3.5 Halpin-Tsai model:

The elastic moduli, shear moduli, and Poisson's ratios of the three-phase CNT/polymer/fiber composite lamina are calculated using the homogenization technique proposed as follows [16],

$$\begin{cases} E_1 = n - l^2 \,/\, k \\ E_2 = 4m(kn - l^2) \,/\, (kn - l^2 + mn) \\ \nu_{12} = l \,/\, 2k \\ G_{12} = G_{13} = p \\ G_{23} = m \end{cases} \tag{15}$$

In which k, l, m, n, and p are five independent Hill's constants of elastic moduli of the three-phase CNT/polymer/fiber composite materials. The terms of Hill's moduli are defined according to [16].

2.2 FST skew plate

A typical skew laminated plate of length *a* and width *b* is illustrated in Fig. 4. A Cartesian coordinate system is fixed on the midplane of the undeformed plate. (*u,v,w*) are considered the displacement vectors of the plate in the (*x,y,z*) directions.

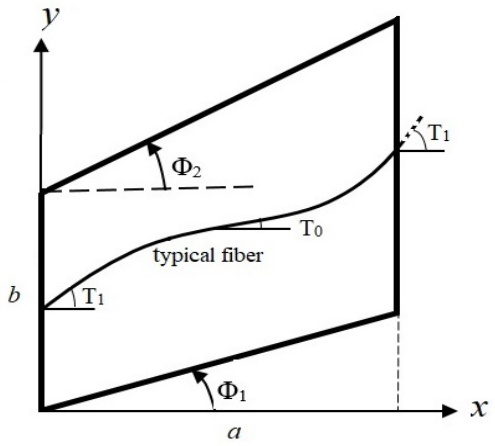

Fig. 4. Typical quadrilateral plate geometry and curvilinear fiber path in the context of the VSCL.

Based on the first shear deformation plate theory, the displacement field on the geometry is approximated as,

$$(u, v, w) = (u_0, v_0, w_0) - z\ (\beta_x, \beta_y, 0) \tag{16}$$

Here, (u_0,v_0,w_0) are the displacements of mid-plane. β_x and β_y are the rotations about *y* and *x* directions at the midplane, respectively. The linear strain vectors are expressed as,

$$\varepsilon = \begin{Bmatrix} \tilde{\varepsilon} \\ \kappa \\ \gamma \end{Bmatrix}$$

$$\tilde{\varepsilon} = \begin{Bmatrix} u^0_{,x} \\ v^0_{,y} \\ u^0_{,y} + v^0_{,x} \end{Bmatrix}, \quad \kappa = \begin{Bmatrix} \beta_{x,x} \\ \beta_{y,y} \\ \beta_{x,y} + \beta_{y,x} \end{Bmatrix}, \gamma = \begin{Bmatrix} w^0_{,x} + \beta_x \\ w^0_{,y} + \beta_y \end{Bmatrix} \tag{17}$$

Where $\tilde{\varepsilon}, \kappa, \gamma$ are the in-plane membrane, bending, and transverse shear strain vectors, respectively. The strain state may be altered into a stress state by using the composite material stiffness transform matrix as,

$$\sigma = \begin{bmatrix} A & B & 0 \\ B & D & 0 \\ 0 & 0 & D_s \end{bmatrix} \varepsilon \tag{18}$$

Here, A, B, D, and D_s are stiffness matrices of extensional, bending-extensional coupling, bending, and transverse shear. The stiffness matrices are calculated through integration over laminate thickness, h, as,

$$\begin{aligned} (A_{ij}(x,y), B_{ij}(x,y), D_{ij}(x,y)) &= \int_{-h/2}^{h/2} \bar{Q}_{ij}(x,y)(1, z, z^2)dz \quad \{i,j=1,2,6\} \\ D_{s\_ij}(x,y) &= \int_{-h/2}^{h/2} \bar{Q}_{ij}(x,y)dz \quad \{i,j=4,5\} \end{aligned} \tag{19}$$

Where $\bar{Q}_{ij}(\mathrm{x}, y)$ are elements of the tow-steered lamina stiffness matrix which are generally assumed to be location-dependent. In the present formulation, any change of fiber curvature along the y-axis is not considered. As a result, the tow-steered lamina stiffness matrix is just a function of x coordination and is defined according to [29]. The fiber orientation inside the CNT-reinforced matrix of the kth layer is assumed to vary linearly in the longitudinal (axial) direction by fiber placement techniques. The fiber orientation angle at an arbitrary position on the geometry is defined linearly as,

$$\theta^k(x) = \frac{(T_e^k - T_m^k)}{a/2} \mid x - \frac{a}{2} \mid + T_m^k \tag{20}$$

Here, T_m^k and T_e^k designate the angle between the fiber and the x-axis at the geometry mid ($x = a/2$) and at the two longitudinal extremes ($x=0,a$), respectively (Fig. 4). The ply fiber orientation corresponding to the fiber placement according to Eq. (20) may be represented by the set $<T_m^k, T_e^k>$. In the case of a conventional constant stiffness lamina with straight fiber reinforcements of angle T^k, the set will appear as

$<T^k, T^k>$. Due to the changing nature of fiber orientation, the lamina equivalent stiffness matrices are a function of the locality. Therefore, the calculations of the stiffness matrices must be performed at every numerical integration point.

2.3 Problem governing equations

In the context of the IGA method, the NURBS functions and their derivatives are utilized as the geometry and displacement field approximation functions. A NURBS basis function of order p (i.e. $R_{i,p}$) on the unit coordination ζ is defined by the weighted average of some B-spline basis functions of the same order as follows [31]:

$$R_{i,p}(\zeta) = \frac{N_{i,p}(\zeta)\ w_i}{\sum_{j=1}^{n} N_{\mathrm{j},p}(\zeta)\ w_j} \tag{21}$$

Where w_j and $N_{\mathrm{j},p}$ are the jth weight coefficient and B-spline constructive of order p. With a given ascending knots vector $[\zeta_1 = 0, \ldots \zeta_i \ldots, \zeta_{n+p+1} = 1]$, the B-spline basis function of order p is defined recursively according to [31]:

$$N_{j,p}(\zeta) = \begin{cases} 1 & \zeta_j \le \zeta < \zeta_{j+1}, p = 0 \\ 0 & otherwise, p = 0 \\ \dfrac{\zeta - \zeta_j}{\zeta_{j+p} - \zeta_j} N_{j,p-1}(\zeta) + \dfrac{\zeta_{j+1+p} - \zeta}{\zeta_{j+1+p} - \zeta_{j+1}} N_{j+1,p-1}(\zeta) & p \ge 1 \end{cases} \tag{22}$$

A NURBS approximation is defined using a set of a defined knot vector and the control points, P_j $(j=1,\ldots,n)$. While utilizing the NURBS approximation in the IGA, the non-zero knot spans $[\zeta_i \le \zeta_{i+1})$ could be

considered the elemental calculation zone. The bivariate NURBS basis approximation functions, corresponding to a NURBS surface, could be defined similarly as,

$$R_{i,j}^{p,q}(\zeta,\eta)=\frac{N_{i,p}(\zeta)M_{j,q}(\eta)\ \ w_{i,j}}{\sum_{i=1}^{n}\sum_{j=1}^{m}N_{i,p}(\zeta)M_{j,q}(\eta)\ \ w_{i,j}}=\frac{N_{i,p}(\zeta)M_{j,q}(\eta)w_{i,j}}{W(\zeta,\eta)} \tag{23}$$

$N_{i,p}$ and $M_{j,q}$ are the B-spline basis of orders p and q defined on their knot vectors in orthogonal directions. A NURBS surface approximation in the plane (ζ,η) is based on a $n\times m$ control point's net of coordination $P_{i,j}$ $(i=1,..,n\ ;\ j=1,...,m)$, as

$$S(\zeta,\eta)=\sum_{i=1}^{n}\sum_{j=1}^{m}R_{i,j}^{p,q}(\zeta,\eta)\mathrm{P}_{i,j} \tag{24}$$

The first directional derivatives of the NURBS basis functions may be derived by applying the quotient rule on Eq. (24), which leads to,

$$\begin{cases}\dfrac{\partial R_{i,j}^{p,q}(\zeta,\eta)}{\partial\zeta}=w_{i,j}\left(\dfrac{\partial N_{i,p}(\zeta)}{\partial\zeta}M_{j,q}(\eta)\ \ W(\zeta,\eta)-\dfrac{\partial W(\zeta,\eta)}{\partial\zeta}N_{i,p}(\zeta)M_{j,q}(\eta)\right)W^{-2}(\zeta,\eta)\\ \dfrac{\partial R_{i,j}^{p,q}(\zeta,\eta)}{\partial\eta}=w_{i,j}\left(\dfrac{\partial M_{j,q}(\eta)}{\partial\eta}N_{i,p}(\zeta)W(\zeta,\eta)-\dfrac{\partial W(\zeta,\eta)}{\partial\eta}N_{i,p}(\zeta)M_{j,q}(\eta)\right)W^{-2}(\zeta,\eta)\end{cases} \tag{25}$$

Where the directional derivatives of the weighting functions, $W(\zeta,\eta)$, are given by,

$$\begin{cases}\dfrac{\partial W(\zeta,\eta)}{\partial\zeta}=\sum_{i=1}^{n}\sum_{j=1}^{m}\dfrac{\partial N_{i,p}(\zeta)}{\partial\zeta}M_{j,q}(\eta)w_{i,j}\\ \dfrac{\partial W(\zeta,\eta)}{\partial\eta}=\sum_{i=1}^{n}\sum_{j=1}^{m}N_{i,p}(\zeta)\dfrac{\partial M_{j,q}(\eta)}{\partial\eta}w_{i,j}\end{cases} \tag{26}$$

The displacement field on the geometry, *u*, is approximated by a bivariate NURBS-based function, as,

$$u = \sum_{i}^{n} \sum_{j}^{m} R_{i,j}^{p,q}\left(\zeta,\eta\right) q_{i,j} \tag{27}$$

Where $R_{i,j}^{p,q}\left(\zeta,\eta\right)$ are the NURBS bivariate basis functions, and $q_{i,j} =< u_{i,j}\ v_{i,j}\ w_{i,j}\ \beta_{x_{i,j}}\ \beta_{y_{i,j}} >^{T}$ are the vector of unknown degrees of freedom on the control point $P_{i,j}$. At an elemental level, the approximation of the displacement is given by,

$$u^{e} = \sum_{A=1}^{ncp} R_{A}^{e}\left(\zeta,\eta\right) q_{A}^{e} \tag{28}$$

Where *ncp* denotes the total number of control points corresponding to the element. The expression is expressed in matrix form as,

$$u^{e} = \mathbf{R}^{e}\mathbf{q}^{e} = \begin{bmatrix} R & 0 & 0 & 0 & 0 \\ 0 & R & 0 & 0 & 0 \\ 0 & 0 & R & 0 & 0 \\ 0 & 0 & 0 & R & 0 \\ 0 & 0 & 0 & 0 & R \end{bmatrix} \begin{Bmatrix} u_{i,j} \\ v_{i,j} \\ w_{i,j} \\ \beta_{x_{i,j}} \\ \beta_{y_{i,j}} \end{Bmatrix} \tag{29}$$

By the substitution of Eq. (29) into Eq. (17), the following strain vector is obtained,

$$\varepsilon^e = \begin{bmatrix} R_{,x} & 0 & 0 & 0 & 0 \\ 0 & R_{,\mathrm{y}} & 0 & 0 & 0 \\ R_{,\mathrm{y}} & R_{,x} & 0 & 0 & 0 \\ 0 & 0 & 0 & R_{,x} & 0 \\ 0 & 0 & 0 & 0 & R_{,\mathrm{y}} \\ 0 & 0 & 0 & R_{,\mathrm{y}} & R_{,x} \\ 0 & 0 & R_{,x} & R & 0 \\ 0 & 0 & R_{,y} & 0 & R \end{bmatrix} q^e \tag{30}$$

Based on the principle of virtual work, the solution to the free vibration problem is sought through Hamilton's principle. The total energy of the problem is computed using the laminated geometry global kinetic (T) and the internal strain (U) energy components as,

$$\Pi = T - U \tag{31}$$

The total internal strain energy for the entire laminate and the kinetic energy component of the laminate, taking into account the effects of inplane and rotational inertia terms, could be approximated after some simplifications as,

$$\begin{aligned} U &= \frac{1}{2}\int_{\Omega} \boldsymbol{\varepsilon}^{eT} \sigma^e \, d\Omega \\ T &= \frac{1}{2}\rho h \int_{\Omega} \left\{ (\dot{u}^2 + \dot{v}^2 + \dot{w}^2) + h^2 (\dot{\beta}_x^{\,2} + \dot{\beta}_y^{\,2}) / 12 \right\} d\Omega \end{aligned} \tag{32}$$

By substituting the displacement field, strains, and stress vectors into the energy terms, and after minimization of the total energy term concerning the vector of degrees of freedom, the governing equations for the free vibration problem are extracted. To implement the necessary boundary conditions at the model edges, a penalty method is utilized and the stiffness of the proportional degrees of freedom at the edge control points is boosted. In the clamped control points, stiffnesses corresponding to all of the degrees of

freedom are manipulated while in the case of a simply-supported edge, stiffnesses corresponding to the translational degrees of freedom are modified. After implementing the boundary conditions, the governing equation corresponding to the whole geometry may be expressed in matrix form as,

$$M\ \ddot{q} + K\ q = 0 \tag{33}$$

Matrices M and K are the global mass, and structural stiffnesses corresponding to the kinetic and strain energy terms.

3. Results and Discussion

The Isogeometric analysis formulation is developed to investigate the free vibration behavior of curvilinear fiber-reinforced nanocomposite laminated plates.

First, the quality of the reviewed two-phase micromechanical models is evaluated. The mechanical properties of a sample unidirectional (UD) fiber lamina are predicted. Table 1 presents the mechanical properties of the resource components and the two-phase composite (UD lamina) as calculated through different micromechanical models, namely the rule of mixture (Mix I, II), Halpin-Tsai, Hahn, and Mori-Tanaka (M-T). Liu and Huang's experimental properties' measurements [34] are also reported. A comparison shows that the highest misprediction occurs for G_{12} and E_{22} properties. The accuracy of calculating E_{11} and ν_{12} is inside the ±10% margin of the measured data and those are the most accurate predicted properties. The Mori-Tanaka model provides the lowest average error among all the micromechanical models. The Halpin-Tsai and Hahn models are in second place.

Table 1. Measured and predicted properties of AS4/3501-6 UD composite (V_f= 0.6).

	Component properties			UD lamina properties (difference%)				
	fiber	matrix	Measured [34]	Mix I model	Mix II model	Halpin-Tsai model	Hahn model	M-T model
E_{11} (GPa)	225	4.2	126	136.68 (+8.5)	136.68 (+8.5)	136.60 (+8.4)	136.68 (+8.5)	136.70 (+8.5)

E_{22} (GPa)	15	4.2	11	7.39 (-32.8)	7.77 (-29.4)	8.37 (-23.9)	8.05 (-26.8)	8.77 (-20.3)
v_{12}	0.2	0.34	0.28	0.256 (-8.6)	0.256 (-8.6)	0.239 (-14.6)	0.256 (-8.6)	0.253 (-9.6)
G_{12} (GPa)	15	1.567	6.6	3.39 (-95)	3.39 (-95)	4.54 (-61)	4.54 (-61)	4.54 (-61)
G_{23} (GPa)	7	1.567	3.92	2.93 (-34)	2.93 (-34)	3.10 (-28)	3.32 (-20)	3.32 (-20)

In the following case studies, the cubic NURBS basis functions are utilized. The numerical integration inside each NURBS elemental region is performed through a 4x4 Gaussian quadrature method. The mechanical properties of the single-walled carbon nanotubes, the reinforcing fibers, and the polymer matrix are presented in Table 2. In the following, a dimension-less frequency parameter is calculated and given through $\Omega = \omega\left(b/\pi\right)^2\sqrt{12(1-\upsilon_m^2)\rho_m/E_m h^2}$ where ω is the natural frequency.

Table 2. Typical mechanical properties of single-walled carbon nanotubes (CNT), reinforcing fibers, and the polymer matrix.[15]

Mechanical properties	CNT	e-glass fibers $\square_f$	matrix phase $\square_m$
Isotropic Young's modulus (*GPa*), *E*	–	–	10
Longitudinal Young's modulus (*GPa*), E_{11}	649.12	69	–
Transverse Young's modulus (*GPa*), E_{22}	11.27	69	–
Longitudinal Shear modulus (*GPa*), G_{12}	5.13	28.75	–
Poisson's ratio, υ	0.284	0.2	0.3
Density (kg/m^3) , ρ	1400	1200	1150

The natural frequencies of a cross-ply five-layer CNT reinforced composite laminated square plate (*a/b=1*, *h/a=0.1*) are extracted to evaluate the present computational models. The first four natural frequencies of the fiber-reinforced nanocomposite laminated plate with layup $[(0/90)_2/0]$ for simply-supported (SSSS) and clamped (CCCC) boundary conditions are calculated and presented in Table 3. The CNT volume fraction increases from *0* to *5* percent. The Eshelby-Mori-Tanaka model in CNT-polymer composition level and different micromechanics models in fiber-matrix composition evaluation are utilized.

It shows that applying the Mori-Tanaka micromechanical model leads to the highest frequencies. The Mix I model gives the lower bound values. With an exception in the third mode, the differences are minimized for the clamped panel. This observation shows the effect of boundary conditions on the panel behavior. As the nano reinforcements' content increases, the difference of frequencies drops in all mode numbers. The

CNT content raise means a stiffer matrix. Therefore, it may be noted that as the mechanical properties of the fiber and matrix phases converge, the difference between micromechanical models subsides. Fig. 5 typically illustrates the frequency results of the simply-supported panel from different micromechanical models.

Table 3. The natural frequencies of fiber-reinforced nanocomposite square laminate for various CNT volume fractions ($a/b=1$, $h/a=0.1$, $\eta=\mu=1$, $V_f=0.6$)

V_r	Micromechanical model	SSSS				CCCC			
		1st	2nd	3rd	4th	1st	2nd	3rd	4th
0%	Mix I	2.9974	6.8597	7.7876	10.8347	5.3217	9.5080	10.4628	13.6322
	Mix II	3.0223	6.9486	7.8206	10.9133	5.3635	9.6112	10.5026	13.7185
	Halpin-Tsai	3.1691	7.2780	8.0867	11.5082	5.5543	10.0380	10.9330	14.4410
	Hahn	3.1977	7.3511	8.1612	11.6331	5.6097	10.1603	11.0519	14.6213
	M-T	3.2210	7.4441	8.1927	11.7077	5.6547	10.2747	11.0942	14.7115
	Mix II [15]	3.0224	6.9487	7.8207	10.9135	5.3636	9.6114	10.5029	13.7188
2%	Mix I	3.1641	7.3072	8.1162	11.4903	5.5919	10.1179	10.9778	14.4732
	Mix II	3.1869	7.3886	8.1474	11.5626	5.6311	10.2141	11.0162	14.5543
	Halpin-Tsai	3.3195	7.6771	8.3744	12.0947	5.7911	10.5778	11.3701	15.1802
	Hahn	3.3488	7.7482	8.4549	12.2238	5.8485	10.7003	11.4972	15.3679
	M-T	3.3770	7.8587	8.4941	12.3144	5.9030	10.8376	11.5502	15.4781
	Mix II [15]	3.1864	7.3875	8.1459	11.5595	5.6301	10.2115	11.0129	14.5489
5%	Mix I	3.3792	7.8791	8.5351	12.3258	5.9360	10.8936	11.6144	15.5311
	Mix II	3.3985	7.9486	8.5627	12.3880	5.9703	10.9775	11.6492	15.6023
	Halpin-Tsai	3.5064	8.1711	8.7315	12.8173	6.0852	11.2454	11.9002	16.0846
	Hahn	3.5360	8.2371	8.8198	12.9495	6.1441	11.3647	12.0379	16.2793
	M-T	3.5706	8.3703	8.8695	13.0613	6.2111	11.5320	12.1054	16.4159
	Mix II [15]	3.3974	7.9458	8.5593	12.3803	5.9679	10.9709	11.6412	15.5889

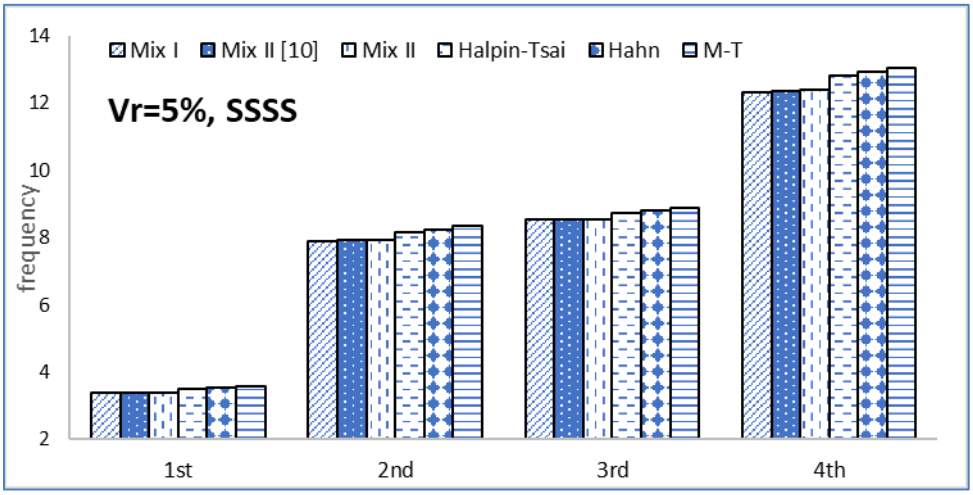

Fig. 5. Comparison of natural frequencies for fiber-reinforced nanocomposite square laminate using various micromechanical models (*SSSS*, $V_r=5\%$)

The natural frequency parameters of a clamped skew nanocomposite are extracted and compared with those from the IMLS-Ritz method as presented in Table 4. No fiber content is assumed (V_f=0%) in the matrix mixture with 11% of uniform and scattered CNT volume content. The results are in very good agreement.

Table 4. The natural frequencies of CNT-reinforced composite skew plate (*clamped, a/b=1*, *h/a=0.01*, $\eta=\mu=1$, V_r=11%, $\Omega = \omega\left(b/\pi\right)^2\sqrt{\rho_m^*/E_m h^2}$)

Skew angle		Mode				
		1	2	3	4	5
Φ=30	Present IGA	4.4261	5.1135	6.5783	8.9034	11.5676
	IMLS-Ritz [36]	4.4368	5.1139	6.5880	8.9181	11.5998
Φ=60	Present IGA	5.8653	8.6927	12.6877	14.0656	17.2340
	IMLS-Ritz [36]	5.8752	8.7733	12.7661	14.1806	17.3403

In the following case studies, the properties of the fiber-matrix composition are evaluated by the Mix II micromechanical model.

The natural frequencies of the cross-ply nanocomposite laminated plate with constant stiffness layup $[(0/90)_2/0]$ are investigated. CNT content of the matrix with volume fractions (V_r) of 0%, 2%, and 5% are considered with possible agglomerations. The three-phase formulation is utilized to evaluate the lamina directional properties. Table 5 and Fig. 6 present the IGA predictions of the fundamental natural frequency of SSSS, CCCC, and SCSC constrained square plates. The results show that higher CNT content strengthens the laminate. But, for large agglomeration sizes ($\mu=0.1$) the strengthening effects are interrupted.

Table 5. Fundamental natural frequency parameters of the nanocomposite laminated plate with various CNT content and mixture quality (*a/b=1, h/a=0.1, V_f=0.6*)

CNT content	(μ,η)		fundamental frequency		
			SSSS	SCSC	CCCC
0%		GDQ, Mix II [15]	3.0224	4.1783	5.3636
		IGA, Mix II	3.0223	4.1782	5.3635
2%	(1,1)	GDQ, Mix II [15]	3.1864	4.4206	5.6301
		IGA, Mix II	3.1869	4.4213	5.6311
	(0.5,1)	GDQ, Mix II [15]	3.1714	4.3986	5.6059
		IGA, Mix II	3.1720	4.3994	5.6071
	(0.1,1)	GDQ, Mix II [15]	3.1081	4.3052	5.5032
		IGA, Mix II	3.1087	4.3061	5.5044
5%	(1,1)	GDQ, Mix II [15]	3.3974	4.7304	5.9679
		IGA, Mix II	3.3985	4.7321	5.9703
	(0.5,1)	GDQ, Mix II [15]	3.3268	4.6271	5.8551
		IGA, Mix II	3.3282	4.6292	5.8579
	(0.1,1)	GDQ, Mix II [15]	3.1416	4.3549	5.5570

IGA, Mix II	3.1426	4.3565	5.5590

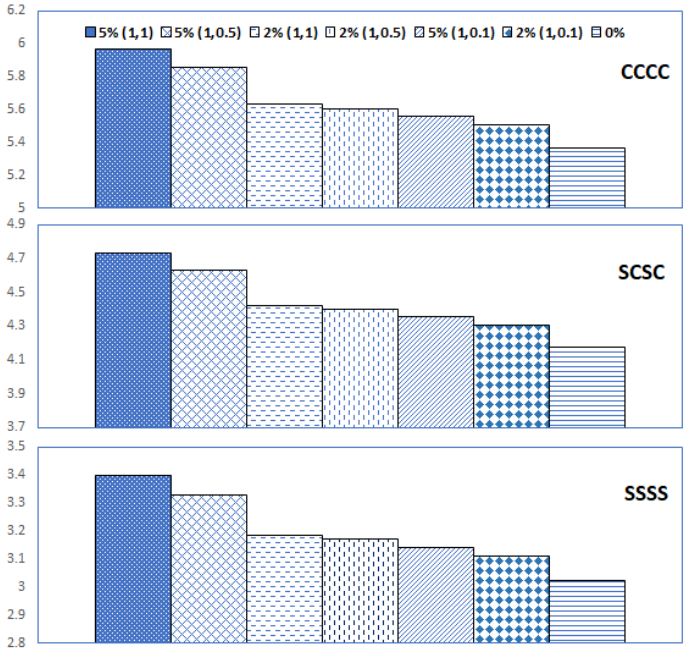

Fig. 6. Fundamental natural frequency parameters of the nanocomposite laminated plate with various CNT content (IGA, Mix II).

The natural frequencies of curvilinear-fiber nanocomposite laminated plates with symmetric layup $[\pm <T_0, T_1>]_S$ are investigated. The CNT content mass fraction (w_r) and fiber orientation angles alter. The fiber orientation angles at the plate longitudinal ends (T_1) and in the middle plate (T_0) are changed from 0- to 90-degrees. The CNT-matrix ideal mixture avoids any possible agglomeration ($\eta=1$, $\mu=1$). The fiber volume fraction of 0.6 is also assumed. The first four natural frequencies of the laminated nano-composite square plate ($a/b=1$, $h/a=0.01$) with CNT content mass fractions (w_r) of *0.0*, *0.1*, and *0.2* are extracted and presented in Table 6 under clamped boundary conditions. The highest frequencies are obtained as fiber angles T_0 and T_1 approach 90- and 0-degree orientations. In the case of the second mode, the best layup is found when T_0 and T_1 come close to 45- and 30-degrees. As the CNT weight ratio grows, the most significant frequency boost is observed in the second mode. The matrix characteristics are not dominant in the third mode since the lowest frequency change is noticed.

Table 6. Natural frequency parameters of clamped CNT-reinforced VSCL square plates
(*a/b=1, h/a=0.01, V_f=0.6, η=μ=1)*

	T_1 variation	natural frequency				T_0 variation	natural frequency			
W_r	layup	mode 1	mode 2	mode 3	mode 4	layup	mode 1	mode 2	mode 3	mode 4
0	$[\pm<45, 0>]_s$	6.169	11.558	13.466	18.237	$[+< 0,45>]_s$	5.830	11.016	12.863	17.496
	$[\pm<45,15>]_s$	6.153	11.696	13.191	18.232	$[+<15,45>]_s$	5.861	11.181	12.684	17.643
	$[\pm<45,30>]_s$	6.073	11.768	12.808	18.151	$[+<30,45>]_s$	5.903	11.440	12.531	17.870
	$[\pm<45,45>]_s$	5.975	11.703	12.521	18.039	$[+<45,45>]_s$	5.975	11.703	12.521	18.039
	$[\pm<45,60>]_s$	5.904	11.512	12.463	17.949	$[+<60,45>]_s$	6.077	11.678	12.905	18.081
	$[\pm<45,75>]_s$	5.872	11.350	12.526	17.908	$[+<75,45>]_s$	6.180	11.492	13.452	18.039
	$[\pm<45,90>]_s$	5.862	11.250	12.630	17.915	$[+<90,45>]_s$	6.235	11.352	13.826	18.049
0.1	$[\pm<45, 0>]_s$	7.032	13.799	14.834	21.045	$[+< 0,45>]_s$	6.849	13.524	14.494	20.593
	$[\pm<45,15>]_s$	7.025	13.872	14.685	21.062	$[+<15,45>]_s$	6.867	13.607	14.400	20.710
	$[\pm<45,30>]_s$	6.982	13.910	14.474	21.031	$[+<30,45>]_s$	6.891	13.740	14.321	20.873
	$[\pm<45,45>]_s$	6.930	13.876	14.318	20.979	$[+<45,45>]_s$	6.930	13.876	14.318	20.979
	$[\pm<45,60>]_s$	6.892	13.780	14.283	20.931	$[+<60,45>]_s$	6.983	13.862	14.524	20.979
	$[\pm<45,75>]_s$	6.875	13.699	14.311	20.900	$[+<75,45>]_s$	7.035	13.765	14.815	20.916
	$[\pm<45,90>]_s$	6.868	13.649	14.361	20.889	$[+<90,45>]_s$	7.061	13.692	15.015	20.882
0.2	$[\pm<45, 0>]_s$	7.644	15.314	15.852	22.943	$[+< 0,45>]_s$	7.549	15.175	15.673	22.700
	$[\pm<45,15>]_s$	7.641	15.352	15.774	22.958	$[+<15,45>]_s$	7.559	15.217	15.624	22.768
	$[\pm<45,30>]_s$	7.619	15.371	15.664	22.946	$[+<30,45>]_s$	7.572	15.285	15.584	22.861
	$[\pm<45,45>]_s$	7.592	15.354	15.583	22.920	$[+<45,45>]_s$	7.592	15.354	15.583	22.920
	$[\pm<45,60>]_s$	7.573	15.305	15.564	22.894	$[+<60,45>]_s$	7.619	15.346	15.689	22.916
	$[\pm<45,75>]_s$	7.563	15.265	15.578	22.875	$[+<75,45>]_s$	7.645	15.297	15.839	22.873
	$[\pm<45,90>]_s$	7.560	15.239	15.602	22.866	$[+<90,45>]_s$	7.657	15.260	15.942	22.846

The natural frequency behavior of the same VSCL nanocomposite plate is investigated as the fiber volume fraction (V_f) changes. The fiber volume fractions of *0.6*, *0.7,* and *0.8* are considered. The simply-supported and clamped geometries are analyzed. A constant fiber mid orientation T_0 and a varying T_1 with a CNT mass fraction (w_r) of 0.15 are assumed. Table 7 presents the natural frequency parameters of the CNT-reinforced VSCL plate overlooking any probable CNT agglomeration.

It is observed that for every 0.1 increase in fiber volume fraction, a uniform 5% frequency boost is obtained in all mode and boundary conditions. The results also show that the highest frequencies may be obtained in the simply-supported case for T_1=45. An exception is also observed in the third mode, where a 0-degree fiber orientation is preferred. The frequency trends in the clamped plate are different. In this case, T_1 angles

of 0-degrees (in the first, third, and fourth modes) and 30-degrees (in the second mode) provide the highest frequencies.

Table 7. Natural frequency parameters of simply-supported and clamped CNT-reinforced VSCL square plates ($a/b=1$, $h/a=0.01$, $w_r=0.15$, $\eta=\mu=1$)

V_f	layup	simply-supported				clamped			
		mode 1	mode 2	mode 3	mode 4	mode 1	mode 2	mode 3	mode 4
0.6	$[\pm<45, 0>]_s$	3.974	9.745	10.292	15.996	7.361	14.620	15.374	22.069
	$[\pm<45,15>]_s$	4.012	9.819	10.254	16.079	7.356	14.673	15.265	22.086
	$[\pm<45,30>]_s$	4.054	9.897	10.224	16.187	7.324	14.700	15.110	22.067
	$[\pm<45,45>]_s$	4.072	9.928	10.193	16.241	7.286	14.676	14.997	22.030
	$[\pm<45,60>]_s$	4.054	9.887	10.160	16.195	7.259	14.607	14.971	21.994
	$[\pm<45,75>]_s$	4.011	9.804	10.129	16.083	7.246	14.549	14.991	21.969
	$[\pm<45,90>]_s$	3.973	9.732	10.121	15.989	7.241	14.513	15.026	21.958
0.7	$[\pm<45, 0>]_s$	4.177	10.266	10.776	16.803	7.723	15.386	16.089	23.165
	$[\pm<45,15>]_s$	4.213	10.335	10.740	16.883	7.718	15.435	15.988	23.182
	$[\pm<45,30>]_s$	4.252	10.408	10.713	16.986	7.689	15.461	15.843	23.165
	$[\pm<45,45>]_s$	4.269	10.438	10.684	17.036	7.654	15.438	15.737	23.131
	$[\pm<45,60>]_s$	4.252	10.400	10.653	16.993	7.628	15.375	15.713	23.098
	$[\pm<45,75>]_s$	4.212	10.322	10.624	16.886	7.617	15.322	15.731	23.074
	$[\pm<45,90>]_s$	4.176	10.255	10.616	16.797	7.612	15.289	15.763	23.062
0.8	$[\pm<45, 0>]_s$	4.407	10.874	11.292	17.709	8.123	16.268	16.847	24.380
	$[\pm<45,15>]_s$	4.437	10.930	11.264	17.777	8.119	16.309	16.763	24.397
	$[\pm<45,30>]_s$	4.470	10.991	11.242	17.865	8.095	16.329	16.644	24.384
	$[\pm<45,45>]_s$	4.484	11.016	11.218	17.907	8.066	16.311	16.556	24.356
	$[\pm<45,60>]_s$	4.470	10.985	11.192	17.869	8.045	16.260	16.536	24.329
	$[\pm<45,75>]_s$	4.437	10.920	11.167	17.780	8.036	16.217	16.551	24.308
	$[\pm<45,90>]_s$	4.406	10.865	11.160	17.705	8.032	16.190	16.577	24.297

The fundamental natural frequency parameter of the CNT-reinforced VSCL skew plate ($\Phi_1=\Phi_2=\Phi$) is extracted as the panel aspect ratio changes. The skew angle of 30 degrees and symmetric variable stiffness layup of $[\pm<45,T_1>]_s$ with diverse T_1 angles are considered. A partially agglomerated CNT-matrix mixture quality of $(\mu,\eta)=(0.5,0.75)$ is assumed. The fundamental frequency of panel aspect ratios (a/b) of *0.5*, *1.0*, and *2.0* under different boundary conditions are extracted. The fundamental natural frequency parameters are presented in Table 8 for different layups, aspect ratios, and boundary conditions. The results show that as the aspect ratio rises, the natural frequency of the panel sharply reduces. The most and the least aspect ratio sensitivity are observed in cases of FCFC and CFCF models, respectively. The panel frequency is affected by the aspect ratio and layup variables are analogous manners in the cases of SSSS and CCCC models. It is also found that the layup parameter T_1 is slightly more effective and frequency-improving in higher aspect ratios.

Table 8. Fundamental natural frequency parameter of CNT-reinforced VSCL skew plates of various aspect ratios.
($h/a=0.01$, $w_r=0.15$, $V_f=0.6$, $(\mu,\eta)=(0.5,0.75)$, $\Phi=30$, $[\pm\langle 45,T_1\rangle]_s$)

boundary conditions	a/b	$T_1=0$	$T_1=15$	$T_1=30$	$T_1=45$	$T_1=60$	$T_1=75$	$T_1=90$
SSSS	0.5	11.111	11.039	11.000	10.979	10.947	10.888	10.823
	1	4.272	4.274	4.300	4.331	4.346	4.337	4.317
	2	2.511	2.524	2.546	2.570	2.584	2.590	2.593
SCSS	0.5	14.891	14.746	14.559	14.382	14.249	14.160	14.100
	1	5.038	5.024	5.016	5.011	5.004	4.991	4.974
	2	2.635	2.646	2.662	2.679	2.691	2.696	2.698
CSCS	0.5	13.867	13.830	13.847	13.863	13.833	13.757	13.687
	1	6.755	6.771	6.807	6.840	6.855	6.856	6.861
	2	4.905	4.920	4.945	4.974	5.004	5.037	5.074
SCSC	0.5	20.135	19.900	19.510	19.124	18.872	18.764	18.721
	1	6.115	6.078	6.016	5.956	5.921	5.907	5.897
	2	2.803	2.809	2.816	2.822	2.829	2.834	2.837
CCCS	0.5	17.125	17.012	16.883	16.755	16.639	16.540	16.469
	1	7.279	7.284	7.295	7.304	7.305	7.302	7.304
	2	4.975	4.990	5.011	5.036	5.063	5.093	5.128
CCCC	0.5	21.928	21.717	21.376	21.038	20.807	20.693	20.635
	1	8.079	8.064	8.030	7.995	7.973	7.966	7.967
	2	5.073	5.085	5.099	5.117	5.139	5.166	5.196
CCCF	0.5	8.526	8.534	8.549	8.569	8.599	8.642	8.696
	1	5.554	5.570	5.590	5.623	5.681	5.763	5.852
	2	4.631	4.640	4.655	4.696	4.769	4.861	4.947
CFCF	0.5	7.718	7.737	7.759	7.771	7.783	7.815	7.880
	1	5.344	5.358	5.371	5.394	5.440	5.514	5.600
	2	4.568	4.574	4.587	4.624	4.692	4.782	4.868
FCFC	0.5	15.202	15.073	14.815	14.522	14.294	14.169	14.110
	1	4.347	4.300	4.207	4.103	4.026	3.987	3.972
	2	1.132	1.119	1.093	1.064	1.044	1.035	1.032

The fundamental natural frequency of the CNT-reinforced VSCL skew plate ($\Phi_1=\Phi_2=\Phi$) is extracted for different particle aggregation contents. The symmetric variable stiffness layup of $[\pm\langle T_0,45\rangle]_s$ with diverse T_0 angles from 0 to 90 degrees is considered. The ideal mixture ($\mu=1,\eta=1$), partial agglomerated mixture ($\mu=0.5,\eta=0.75$), and fully agglomerated mixture ($\mu=0.5,\eta=1$) are assumed. The fundamental frequency parameters are presented in Table 9 for altered layups, mixture quality, and boundary conditions.

According to the predicted frequencies, the frequency reduction is a fair result of CNT-matrix poor quality (in terms of mixture parameters). Also, as the skew angle grows, the panel frequencies increase. However, the optimal T_0 fiber angle is different as the plate skew angle changes. This observation is rather noticeable in the case of the simply-supported plate. Fig. 7 depicts the variations of the fundamental frequency

parameters of the skew plates with change in the layup angle for the case of a partial agglomerated mixture. It shows that the boundary conditions affect the behavior of the low skew plate (i.e. Φ=0 and Φ=15).

Table 9. Fundamental natural frequency parameter of CNT-reinforced VSCL skew plates for different layups.
($a/b=1$, $h/a=0.01$, $w_r=0.15$, $V_f=0.6$, $[\pm<T_0,45>]_s$)

(μ,η)	T_0	simply-supported				clamped			
		$\Phi=0$	$\Phi=15$	$\Phi=30$	$\Phi=45$	$\Phi=0$	$\Phi=15$	$\Phi=30$	$\Phi=45$
(1.0,1.0)	0	4.033	4.088	4.400	5.385	7.227	7.389	8.101	10.330
	15	4.048	4.093	4.383	5.334	7.240	7.391	8.090	10.283
	30	4.059	4.102	4.379	5.298	7.258	7.399	8.089	10.262
	45	4.063	4.111	4.385	5.283	7.286	7.417	8.100	10.255
	60	4.059	4.117	4.396	5.285	7.325	7.451	8.125	10.256
	75	4.047	4.118	4.408	5.299	7.361	7.495	8.166	10.273
	90	4.031	4.115	4.421	5.323	7.380	7.534	8.219	10.323
(0.5,0.75)	0	3.990	4.042	4.347	5.320	7.139	7.296	7.996	10.195
	15	4.007	4.047	4.330	5.265	7.153	7.298	7.984	10.144
	30	4.019	4.057	4.325	5.227	7.172	7.307	7.984	10.122
	45	4.023	4.067	4.331	5.211	7.203	7.327	7.995	10.114
	60	4.018	4.073	4.343	5.213	7.244	7.364	8.022	10.115
	75	4.005	4.074	4.356	5.227	7.284	7.411	8.066	10.134
	90	3.989	4.071	4.370	5.253	7.304	7.453	8.124	10.188
(0.5,1.0)	0	3.810	3.846	4.124	5.044	6.761	6.898	7.546	9.615
	15	3.831	3.853	4.100	4.970	6.780	6.902	7.530	9.547
	30	3.847	3.866	4.094	4.919	6.805	6.912	7.529	9.517
	45	3.852	3.878	4.102	4.897	6.846	6.939	7.545	9.506
	60	3.845	3.886	4.117	4.899	6.902	6.988	7.580	9.507
	75	3.829	3.886	4.134	4.918	6.957	7.052	7.639	9.532
	90	3.807	3.884	4.153	4.952	6.985	7.111	7.717	9.604

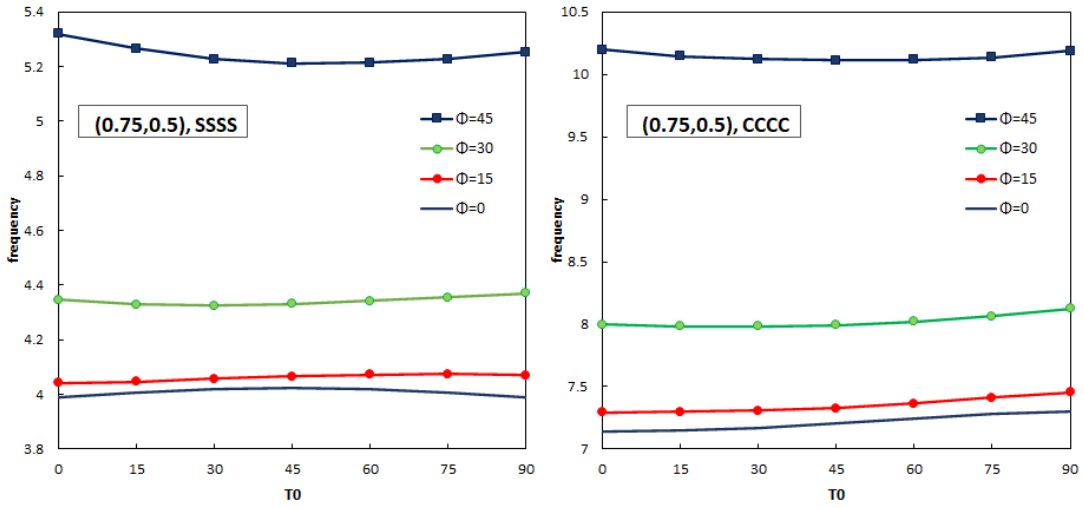

Fig. 7. Fundamental natural frequency coefficients of CNT-reinforced VSCL skew plates
($a/b=1$, $h/a=0.01$, $w_r=0.15$, $V_f=0.6$, $(\mu,\eta)=(0.5,0.75)$, $[\pm<T_0,45>]_s$)

The effects of the CNT agglomeration on the natural frequencies of the CNT-reinforced VSCL skew plate ($\Phi_1=\Phi_2=\Phi$) are investigated. Symmetric VSCL with layup $[\pm<30,45>]_s$ and different plate skew angles are considered. The consequences of changing the agglomeration parameters on the natural frequencies are studied. Fig. 8 depicts the fundamental frequencies in the plate skew angles under consideration as the agglomeration indices alter.

The results show that for the case of a constant CNT-matrix mixture index η of 0.9 as μ grows, the panel frequency increases smoothly. The rate of the panel stiffening (in terms of the frequency growth) is lower for higher μ but is found to be higher than 15 percent. On the other hand, the agglomeration stiffening effect is more significant for higher plate skew angles. This evidence is especially major in the cases of simply-supported models. This observation shows that for a constant agglomerated CNTs fraction, the bigger the clumps are, the more the reinforcement will be. For an unchanging μ parameter of *0.5*, as the agglomeration parameter η grows from 0.5 to 1.0, the fundamental frequency slightly reduces. The greater η means a higher portion of the CNT contents is clustered together such that for $\eta=1$, all CNT content is agglomerated. The reduction rates are roughly the same for all the skew angle sets. This fact reveals that as the agglomerated spots get bulkier and the scattered CNT volume lessens, the matrix reinforcing quality becomes poor.

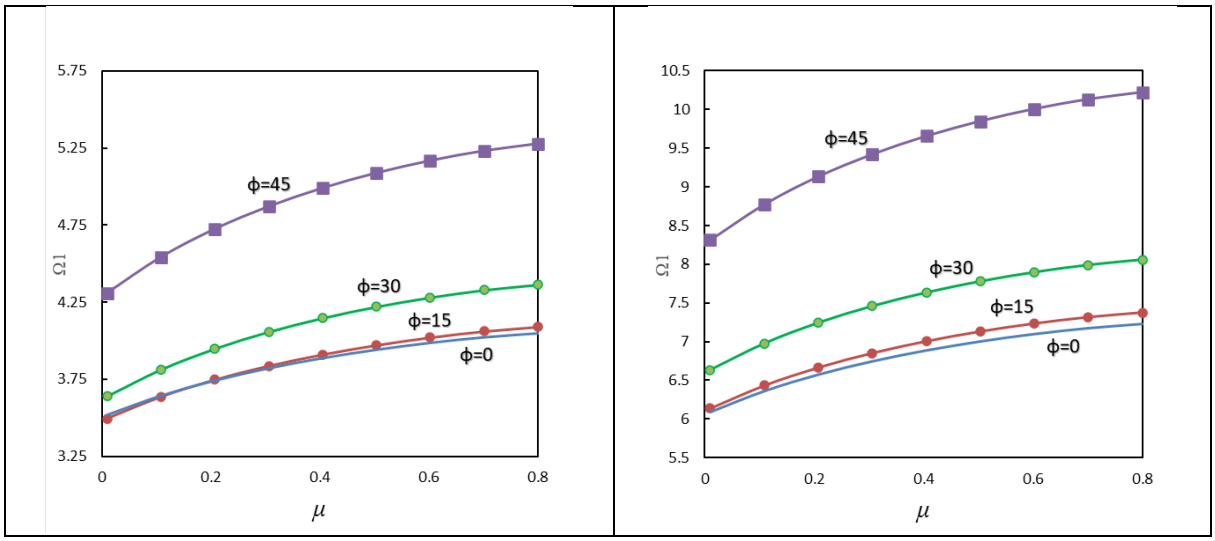

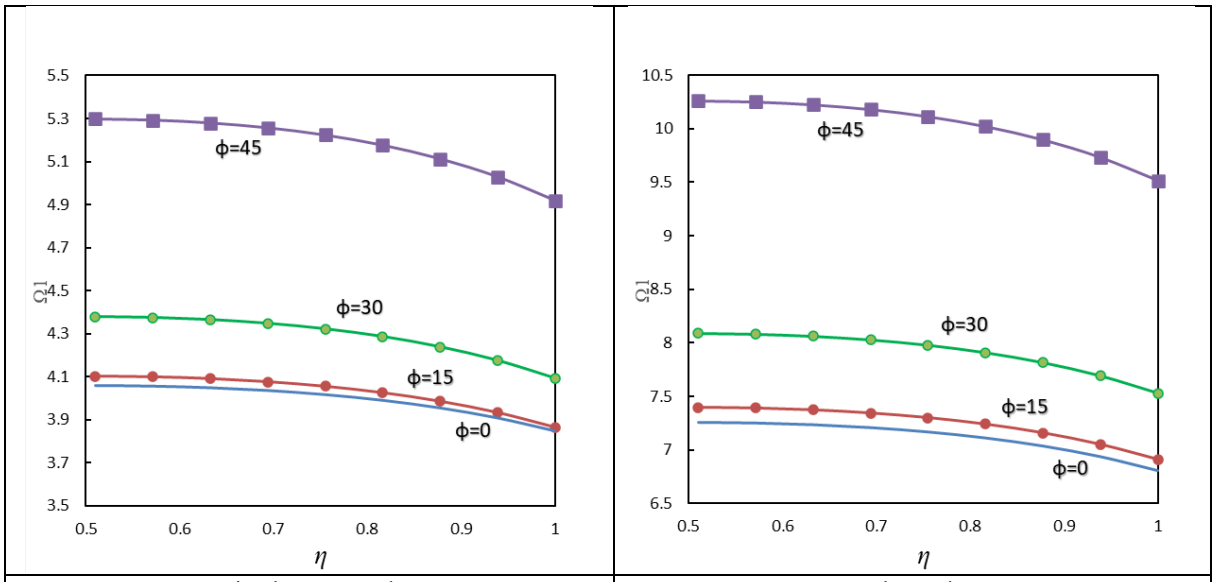

Fig. 8. Fundamental natural frequency coefficient of CNT-reinforced VSCL skew plates with different mixture and boundary condition properties. ($a/b=1$, $h/a=0.01$, $w_r=0.15$, $V_f=0.6$, $[\pm<30,45>]_s$)

The effects of the CNT agglomeration and curvilinear layup are studied on the free vibration of the CNT-reinforced VSCL quadrilateral plates. The plate planform is given by two side obliqueness of $(\Phi 1, \Phi 2)$. The plate edge constraints according to CSCS are assumed. Table 10 presents the fundamental frequencies of the quadrilateral plates of various planform and layups. It shows that the mixture quality and fiber orientation act analogous in all geometry cases. The minimum frequency is found in the cases with planforms (0,0) and (10,10). On the other hand, the highest frequencies (around 40% higher than the square planform) are achieved in the trapezoidal plan of (20,-10), which comparatively has the minimum plate area. This difference is found independent of layup and mixture quality.

Table 10. Fundamental natural frequency parameter of CNT-reinforced VSCL quadrilateral plates for different layups and mixture qualities. ($a/b=1$, $h/a=0.01$, $w_r=0.15$, $V_f=0.6$, $[\pm<T_0,45>]_s$)

(μ,η)	(Φ_1,Φ_2)	T_0 0	15	30	45	60	75	90
(1.0,1.0)	(0, 0)	5.774	5.796	5.830	5.884	5.953	6.022	6.067
	(10,10)	5.858	5.872	5.897	5.939	6.002	6.075	6.137
	(0,10)	6.661	6.684	6.722	6.785	6.873	6.968	7.040
	(10,-10)	7.840	7.872	7.929	8.017	8.130	8.240	8.313
	(20,-10)	9.518	9.545	9.600	9.689	9.802	9.918	10.005

(0.5,0.75)	(0, 0)	5.699	5.723	5.760	5.818	5.893	5.968	6.016
	(10,10)	5.781	5.796	5.823	5.869	5.937	6.015	6.082
	(0,10)	6.572	6.596	6.637	6.706	6.801	6.903	6.981
	(10,-10)	7.734	7.769	7.831	7.926	8.048	8.166	8.245
	(20,-10)	9.390	9.419	9.479	9.575	9.697	9.822	9.916
(0.5,1.0)	(0, 0)	5.380	5.412	5.462	5.540	5.640	5.741	5.806
	(10,10)	5.447	5.468	5.504	5.566	5.657	5.763	5.853
	(0,10)	6.186	6.219	6.274	6.367	6.494	6.632	6.737
	(10,-10)	7.278	7.327	7.410	7.538	7.701	7.860	7.965
	(20,-10)	8.834	8.875	8.957	9.087	9.252	9.417	9.541

Concluding remarks

A numerical model is introduced for frequency prediction of the tow-steered three-phase CNT/polymer/fiber composition. The free vibration behavior of the three-phase curvilinear-fiber/CNT/polymer composite laminated quadrilateral plates subjected to various sets of boundary conditions is studied. Numerical solutions are obtained utilizing a first-order shear deformation NURBS-based isogeometric analysis formulation. The Eshelby-Mori-Tanaka scheme predicts the consequent properties of the CNT/polymer blend. As the CNT additive clustering may occur during the nanocomposite blending, different CNT agglomeration levels are considered. The mechanical properties of the curvilinear fiber/matrix laminate are estimated by some micromechanics homogenizing theories. The effect of fiber and CNT content and the mixture quality on the structural frequencies is discussed.

The M-T model is found to provide good equivalent properties of the fiber-matrix composition. But, none of the implemented micromechanical models can well-predict the equivalent modulus of shear and transverse elasticities. Using the M-T model offers higher natural frequencies and the Mix I model gives the minimum frequencies. This difference is reduced as the CNT content grows. Furthermore, as the CNT weight ratio grows, the most significant frequency boost is observed in the second natural mode of the square plate. Increasing the CNT content (in terms of *Vr*) rises the panel frequency, but the occurrence of larger agglomeration spots can neutralize this effect. For every *0.1* increase of the fiber volume fraction, a uniform *5%* frequency boost is observed in all boundary conditions. The frequency trends of the simply-supported and clamped conditions are generally different. As the plate aspect ratio rises, the natural

frequencies of the skew laminate sharply fall. The most and the least aspect ratio effects are observed in cases of FCFC and CFCF skew plates, respectively. The sensitivity of the skew panel frequency to the aspect ratio and layup properties is analogous in the cases of simply-supported and clamped models. It is also found that the layup parameter *T1* is slightly more effective and frequency-improving in higher aspect ratios. The results indicate that as the agglomerated spots get bulkier and the scattered unique CNTs lessen, the matrix reinforcing quality is undermined. The level of the panel stiffening (in terms of the frequency growth) is lower for higher μ. For higher plate skew angles, the agglomeration stiffening effect is more significant.

References

[1] A.J. Rodriguez, M.E. Guzman, C.-S. Lim, B. Minaie, Mechanical properties of carbon nanofiber/fiber-reinforced hierarchical polymer composites manufactured with multiscale-reinforcement fabrics, Carbon 49(3): 937-948, 2011.

[2] Z. Han, A. Finab, Thermal conductivity of carbon nanotubes and their polymer nanocomposites: A review, Progress in Polymer Science 36(7): 914-944, 2011.

[3] Y. Rao, H.-L. Dai, and T. Dai, Linkages among fiber content, porosity and local aggregation in fiber-reinforced composites and their effect on effective properties, Journal of Materials Science 52(20): 12486-505, 2017.

[4] M. Strozzi, V.V. Smirnov, L.I. Manevitch, F. Pellicano, Nonlinear vibrations and energy exchange of single-walled carbon nanotubes. Radial breathing modes, Journal of Sound and Vibration 381: 156-178, 2016

[5] H.-L. Dai, Z.-W. Huang, C. Mei, Z.-Y. Lin, Prediction of the tensile strength of hybrid polymer composites filled with spherical particles and short fibers, Composite Structures 187: 509-517, 2018.

[6] M. Strozzi and F. Pellicano, Nonlinear resonance interaction between conjugate circumferential flexural modes in single-walled carbon nanotubes, Nonlinear Vibration of Continuous Systems 2019: 3241698, 2019.

[7] T. Dai, Y. Yang, H.-L. Dai, H. Tang, Z.-Y. Lina, Hygrothermal mechanical behaviors of a porous FG-GRC annular plate with variable thickness considering aggregation of CNTs, Composite Structures 215: 198-213, 2019.

[8] Z.-W. Huang, Q.-F. Gui, H.-L. Dai, Investigation on microscale hygrothermal behavior of carbon nanotube-reinforced polymer composite, Polymer Composites 41: 3421-3433, 2020.

[9] Y. Yang, Q. He, Y. Rao, H.-L. Dai, Estimation of dynamic thermo viscoelastic moduli of short-fiber-reinforced polymers based on a micromechanical model considering interphases/interfaces conditions, Polymer Composites 41: 788-803, 2020.

[10] M. Heshmati and M.H. Yas, Free vibration analysis of functionally graded CNT-reinforced nanocomposite beam using Eshelby-Mori-Tanaka approach. J. Mechanical Science and Technology 27: 3403, 2013.

[11] G. Bhardwaj, A.K. Upadhyay, R. Pandey, K.K. Shukla, Nonlinear flexural and dynamic response of CNT reinforced laminated composite plates. Composites Part B: Engineering 45: 89-100, 2013.

[12] M. Rafiee, X.F. Liu, X.Q. He, S. Kitipornchai, Geometrically nonlinear free vibration of shear deformable piezoelectric carbon nanotube/fiber/polymer multi-scale laminated composite plates. Journal of Sound and Vibration 333 (14): 3236-3251, 2014.

[13] Y. Kiani, Free vibration of FG-CNT reinforced composite skew plates, Aerospace Science and Technology 58: 178-188, 2016.

[14] M.M. Ardestani, L.W. Zhang, K.M. Liew, Isogeometric analysis of the effect of CNT orientation on the static and vibration behaviors of CNT-reinforced skew composite plates. Computational Methods Applied Mechanical Engineering 317: 341-379, 2017.

[15] S. Kamarian, M. Shakeri, M. H. Yas, Natural frequency analysis and optimal design of CNT/fiber/polymer hybrid composites plates using Mori-Tanaka approach, GDQ technique and Firefly algorithm. Polymer Composites 39(5): 1433-1446, 2018.

[16] F. Tornabene, M. Bacciocchi, N. Fantuzzi, J. Reddy, Multiscale approach for three-phase CNT/polymer/fiber laminated nanocomposite structures. Polymer Composites 40 (S1): E102-E126, 2019.

[17] F. Tornabene, N. Fantuzzi, M. Bacciocchi, Linear static response of nanocomposite plates and shells reinforced by agglomerated carbon nanotubes. Composites Part B: Engineering 115: 449-476, 2017.

[18] A.R. Ghasemi, M. Mohandes, R. Dimitri, F. Tornabene, Agglomeration effects on the vibrations of CNTs/ fiber/polymer/metal hybrid laminates cylindrical shell. Composites Part B: Engineering 167: 700-716, 2019.

[19] A.H. Yousefi, P. Memarzadeh, H. Afshari, S.J. Hosseini, Agglomeration effects on free vibration characteristics of three-phase CNT/polymer/fiber laminated truncated conical shells. Thin-Walled Structures 157: 107077, 2020.

[20] S.K. Georgantzinos, P.A. Antoniou, G.I. Giannopoulos, A. Fatsis, and S.I. Markolefas, Design of laminated composite plates with carbon nanotube inclusions against buckling: waviness and agglomeration effects, Nanomaterials 11: 2261, 2021.

[21] F. Heidari, K. Taheri, M. Sheybani, M. Janghorban, and A. Tounsi, On the mechanics of nanocomposites reinforced by wavy/defected/aggregated nanotubes. Steel and Composite Structures, An International Journal 38(5): 533-545, 2021.

[22] D.S. Craveiro, M.A.R. Loja, An assessment of thick nanocomposite plates' behavior under the influence of carbon nanotubes agglomeration, J. Composites Science. 5: 41, 2021.

[23] E.C. Demir, A. Benkaddour, D.R. Aldrich, M.T. McDermott, C.I. Kim, and C. Ayranci, A predictive model towards understanding the effect of reinforcement agglomeration on the stiffness of nanocomposites, Journal of Composite Materials, 2022

[24] H. Akhavan, P. Ribeiro, Natural modes of vibration of variable stiffness composite laminates with curvilinear fibers. Composite Structures 93(11): 3040-3047, 2011.

[25] F. Tornabene, N. Fantuzzi, M. Bacciocchi, E. Viola, Higher-order theories for the free vibrations of doubly curved laminated panels with curvilinear reinforcing fibers by means of a local version of the GDQ method, Composites Part B: Engineering 81:196-230, 2015.

[26] G.G. Lozano, A. Tiwari, C. Turner, S. Astwood, A review on design for manufacture of variable stiffness composite laminates. Proceedings of the Institution of Mechanical Engineers, Part B: Journal of Engineering Manufacture 230 (6): 981-992, 2016.

[27] P. Hao, C. Liu, X. Liu, X. Yuan, B. Wang, G. Li, M. Dong, and L. Chen, Isogeometric analysis and design of variable-stiffness aircraft panels with multiple cutouts by level set method, Composite Structures 206: 888-902, 2018.

[28] P. Hao, X. Yuan, C. Liu, B. Wang, H. Liu, G. Li, and F. Niu, An integrated framework of exact modeling, isogeometric analysis and optimization for variable-stiffness composite panels. Computational Methods in Applied Mechanical Engineering 339: 205-238, 2018.

[29] V. Khalafi and J. Fazilati, Isogeometric panel flutter analysis of variable stiffness composite laminated skew panels subjected to yawed flow. Journal of Fluids and Structures 82: 198-214, 2018.

[30] V. Khalafi and J. Fazilati, Parametric instability behavior of tow steered laminated quadrilateral plates using isogeometric analysis. Thin-Walled Structures 133: 96-105, 2018.

[31] J. Fazilati and V. Khalafi, Effects of embedded perforation geometry on the free vibration of tow steered variable stiffness composite laminated panels. Thin-Walled Structures, 144, 2019.

[32] Z.-M. Huang, Y.-X. Zhou, Strength of fibrous composites. Springer, 2012.

[33] H. Hahn, Simplified formulas for elastic moduli of unidirectional continuous fiber composites. J. Composite Technology Reviews 2(3): 5-7, 1980.

[34] L. Liu, Z. Huang, A note on Mori-Tanaka's method. Acta Mechanica Solida Sinica 27(3): 234-244, 2014.

[35] D.-L. Shi, X.-Q. Feng, Y.Y. Huang, K.-C. Hwang, H. Gao, The effect of nanotube waviness and agglomeration on the elastic property of carbon nanotube-reinforced composites. J. Engineering Materials and Technology 126 (3): 250-257, 2004.

[36] L.W. Zhang, On the study of the effect of in-plane forces on the frequency parameters of CNT-reinforced composite skew plates, Composite Structures 160: 824-837, 2017.